Optics Communications 283 (2010) 1338–1345

Contents lists available at ScienceDirect

Optics Communications

journal homepage: www.elsevier.com/locate/optcom

Symmetries and asymmetries in coherent atomic excitation by chirped laser pulses

B.T. Torosov [a,b,*], G.S. Vasilev [b,c], N.V. Vitanov [b,d]

[a] School of Physics and Astronomy, University of Leeds, Leeds LS2 9JT, United Kingdom
[b] Department of Physics, Sofia University, James Bourchier 5 Blvd., 1164 Sofia, Bulgaria
[c] Department of Physics, University of Oxford, Parks Road, Oxford OX1 3PU, United Kingdom
[d] Institute of Solid State Physics, Bulgarian Academy of Sciences, Tsarigradsko Chaussée 72, 1784 Sofia, Bulgaria

ARTICLE INFO

Article history:
Received 25 October 2009
Received in revised form 20 November 2009
Accepted 20 November 2009

ABSTRACT

We analyze the effects of laser-induced Stark shift and irreversible population loss on the technique of chirped-frequency adiabatic passage, and the ensuing symmetries and asymmetries in the ionization and fluorescence signals. We find that the properties of the detection signal depend critically on the fashion in which it is collected: for example, the post-pulse populations of the ground and excited states, and the ionization signal collected during the excitation, possess different symmetry properties with respect to the frequency chirp rate and the static frequency detuning. We illustrate these features with two exactly soluble analytic models, which describe simultaneous excitation and ionization of a two-state quantum system, as it typically occurs in atomic excitation with femtosecond laser pulses. We find that the ionization signal may exhibit unexpected oscillations and derive the conditions for maximizing their contrast.

1. Introduction

Coherent excitation of a two-state atom by a laser pulse is usually associated with symmetric excitation profiles [1], i.e. the excitation probability is a symmetric (even) function of the detuning Δ and the chirp rate C. When multiple states are involved, there is always a multitude of (often interfering) excitation pathways, and a change of sign in the detuning or the chirp of the excitation pulse (or pulses) makes the system follow a different path in Hilbert space, and arrive at a different outcome. A two-state system, however, is too simple in this respect for it has only one transition path $\psi_1 \leftrightarrow \psi_2$, from which the symmetry of the excitation probability $P_{1\to 2}$ with respect to Δ and C usually, but not always, follows. Symmetries of this sort can be broken, for example, by the presence of dynamic Stark shifts and population losses (e.g., ionization) induced by the excitation pulse.

In this article we examine in some detail the sources of asymmetries in the two-state excitation profiles. We find that the properties of the detected signal depend significantly on its nature: for example, the post-pulse populations of the ground and excited states (probed, e.g., by subsequent laser-induced fluorescence or ionization) and the ionization signal accumulated during the excitation display different symmetry properties with respect to the frequency chirp and the detuning. To this end, we use two analytically exactly soluble models, which extend the analytic models of Demkov–Kunike [2] and Carroll–Hioe [3] to complex detuning, which is needed to model simultaneous excitation and population loss. These models allow us to describe the effects of laser-induced Stark shift and irreversible population loss (spontaneous emission, ionization, etc.) upon chirped adiabatic passage techniques; these effects become significant in strong-field atomic excitation by ultrashort (picosecond and femtosecond) laser pulses [4–6].

The paper is organized as follows. We introduce the model physical system in Section 2. The two-state symmetries and asymmetries are described in Section 3. The analytic models are presented and discussed in Section 4. The conclusions are summarized in Section 5.

2. Model physical system

2.1. Two-state system

Our model system comprises two states, ground ψ_1 and excited ψ_2, the transition between which is driven by an external coherent field. The evolution of this system is described by the Schrödinger equation [1]:

$$i\hbar\partial_t \mathbf{c}(t) = \mathbf{H}(t)\mathbf{c}(t), \tag{1}$$

where $\mathbf{c}(t) = [c_1(t), c_2(t)]^T$ is the column vector with the probability amplitudes $c_1(t)$ and $c_2(t)$ of the two states ψ_1 and ψ_2. The Hamiltonian in the rotating-wave approximation reads:

* Corresponding author. Address: Department of Physics, Sofia University, James Bourchier 5 Blvd., 1164 Sofia, Bulgaria.
E-mail address: torosov@phys.uni-sofia.bg (B.T. Torosov).

0030-4018/$ - see front matter © 2009 Elsevier B.V. All rights reserved.
doi:10.1016/j.optcom.2009.11.058

$$\mathbf{H}(t) = \hbar \begin{bmatrix} 0 & \frac{1}{2}\Omega(t) \\ \frac{1}{2}\Omega(t) & \Delta(t) - \frac{1}{2}i\Gamma(t) \end{bmatrix}. \tag{2}$$

The detuning Δ is the offset of the laser carrier frequency ω from the Bohr transition frequency ω_0, $\Delta = \omega_0 - \omega$. The detuning $\Delta(t)$ is real and may have an arbitrary time dependence, which may occur through temporal variation of either the laser frequency $\omega(t)$ (by frequency chirping) or the atomic transition frequency $\omega_0(t)$ (by using controlled Stark or Zeeman shifts induced by time-varying electric or magnetic fields). The Rabi frequency $\Omega(t)$ quantifies the field-induced coupling between the two states. For single-photon electric-dipole excitation, we have $\Omega(t) = -\mathbf{d}\cdot\mathbf{E}(t)/\hbar$, where $\mathbf{d}$ is the atomic transition dipole moment and $\mathbf{E}(t)$ is the envelope of the laser electric-field amplitude. For two-photon excitation, the Rabi frequency is proportional to $\mathbf{E}^2(t)$. This follows from the fact that such processes correspond to second-order terms in perturbation theory [1]. The Rabi frequency $\Omega(t)$ is assumed real, positive and pulse-shaped. The irreversible-loss rate $\Gamma(t)$ is real and positive and may be constant or pulse-shaped. The latter situation, of pulse-shaped $\Gamma(t)$ occurs, for instance, when the driving pulse, while acting upon the transition $\psi_1 \leftrightarrow \psi_2$, simultaneously ionizes the population of the excited state ψ_2; this typically occurs in excitation by femtosecond laser pulses.

We shall be concerned with excitation of a two-state atom by a single intense laser pulse, which may have the following simultaneous actions: (i) excite the transition $\psi_1 \leftrightarrow \psi_2$; (ii) ionize the population from state ψ_2 with a rate $\Gamma(t)$; (iii) induce dynamic Stark shifts caused by the presence of the other, far off-resonance states in the atom. Let the time dependence of the laser electric field be described by the function $f(t)$; hence the laser intensity is $I(t) = I_0 f(t)^2$. Then the Rabi frequency $\Omega(t)$ will be proportional to either $f(t)$ or $f(t)^2$, whereas the dynamic Stark shift $S(t)$ and the ionization rate $\Gamma(t)$ (for one-photon ionization) are both proportional to $f(t)^2$:

$$\Omega(t) = \begin{cases} \Omega_0 f(t) \propto \sqrt{I(t)} & \text{(one-photon transition)}, \\ \Omega_0 f(t)^2 \propto I(t) & \text{(two-photon transition)}, \end{cases} \tag{3a}$$

$$S(t) = S_0 f(t)^2 \propto I(t), \tag{3b}$$

$$\Gamma(t) = \Gamma_0 f(t)^2 \propto I(t). \tag{3c}$$

Since the analytical models that we consider comprise symmetric pulse shapes, unless specified otherwise, we shall assume that the pulse shape $f(t)$ is a symmetric (even) function of time:

$$f(-t) = f(t). \tag{4}$$

However, general results for asymmetric shapes are also derived. The detuning may have a static component Δ_0 and a chirped (time-dependent) part $B(t)$, which may be linear:

$$B(t) = Ct, \tag{5}$$

or nonlinear, e.g., $B(t) = B\tanh(t/T)$.

The dynamic Stark shift is included in the detuning, i.e. we have:

$$\Delta(t) = \Delta_0 + S(t) + B(t). \tag{6}$$

We shall therefore assume that the detuning contains two parts: a symmetric one (even function of time) $\Delta_e = \Delta_0 + S(t)$ and an antisymmetric one (odd function of time) $\Delta_o = B(t)$.

The system is supposed to be initially in state ψ_1 $[c_1(t_i) = 1, c_2(t_i) = 0]$ and we are interested in the occupation probabilities after the interaction, $P_{1\to1} = |c_1(t_f)|^2$ and $P_{1\to2} = |c_2(t_f)|^2$, and the accumulated population loss (ionization) $P_{\text{ion}} = 1 - P_{1\to1} - P_{1\to2}$.

2.2. Detection signals

In a two-state system, the detection signal may be measured by at least three different scenarios.

- Measurement of the *post-pulse population* of the excited state ψ_2 (the transition probability $P_{1\to2}$) via fluorescence from this state or probe-pulse ionization, Fig. 1(a).
- Measurement of the *post-pulse population* of the initial state ψ_1 (the survival probability $P_{1\to1}$) by using a probe laser pulse to an auxiliary excited state and the ensuing fluorescence or ionization from this state, Fig. 1(b).
- Measurement of the ionization signal P_{ion} from the excited state ψ_2, caused by the excitation pulse itself, and therefore collected *during* the excitation, Fig. 1(c).

In this paper we show that the three signals $P_{1\to1}$, $P_{1\to2}$ and P_{ion} may contain different information, for example, they may have different symmetry properties. It is therefore very important in an experiment, even for such a simple two-state system, to pay attention to *how* the signal has been collected.

3. Asymmetries in two-state excitation

The time-dependent two-state quantum system possesses various symmetries. We shall now describe some cases when asymmetries emerge, and then analyze what can be accomplished by means of chirped pulses.

In the numerical simulations below we use symmetric $f_s(t)$ and asymmetric $f_a(t)$ pulse shapes:

$$f_s(t) = \mathrm{e}^{-t^2/T^2}, \tag{7a}$$

$$f_a(t) = \mathrm{e}^{-t^2/T^2}[1 + \tanh(t/T)]/2. \tag{7b}$$

The Rabi frequency and the Stark shift are taken as

$$\Omega(t) = \Omega_0 f_{s,a}(t), \tag{7c}$$

$$S(t) = s\Omega(t) = S_0 f_{s,a}(t), \tag{7d}$$

with $S_0 = s\Omega_0$.

3.1. Sign inversion symmetries in a two-state system

3.1.1. Sign inversion of the detuning and the Rabi frequency

In the lossless case ($\Gamma = 0$), the sign flip in the detuning $\Delta(t) \to -\Delta(t)$ is equivalent to a complex conjugation of both $c_1(t)$ and $c_2(t)$, and a change of sign in the amplitude $c_1(t)$. Neither of these operations change the transition probability, which is therefore

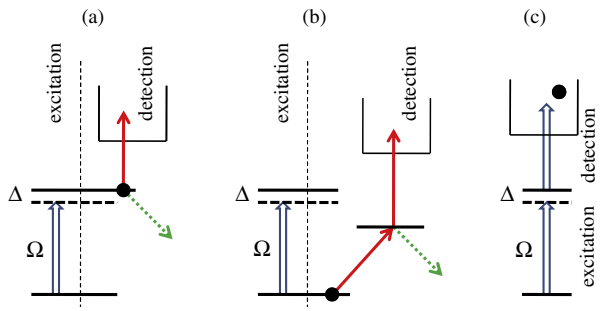

Fig. 1. Different approaches to measure the detection signal in a two-state system, as explained in Section 2.2: (a) post-pulse population of the excited state ψ_2 probed by a subsequent fluorescence or laser-induced ionization; (b) post-pulse population of the initial state ψ_1 probed by a subsequent laser-induced fluorescence or ionization; (c) ionization signal P_{ion} from the excited state ψ_2, caused by the excitation pulse itself.

invariant to the sign flip of the detuning. The presence of losses ($\Gamma > 0$) does not change these arguments because the above operations do not change the sign of the Γ-term.

The sign flip of the Rabi frequency $\Omega(t) \to -\Omega(t)$ is equivalent to the sign flip $c_2(t) \to -c_2(t)$, and hence this operation does not alter the probabilities either. Again, this conclusion does not depend on the presence of losses.

3.1.2. Time inversion

In the lossless case ($\Gamma = 0$), the probabilities are invariant upon time inversion. This feature follows from the following arguments. The propagator $\mathbf{U}(t_f, t_i)$ from the initial time t_i to the final time t_f is defined via:

$$\mathbf{c}(t_f) = \mathbf{U}(t_f, t_i)\mathbf{c}(t_i). \tag{8}$$

Time inversion means to propagate from t_f to t_i, which occurs through the inverse of the propagator:

$$\mathbf{c}(t_i) = \mathbf{U}^{-1}(t_f, t_i)\mathbf{c}(t_f) = \mathbf{U}^{\dagger}(t_f, t_i)\mathbf{c}(t_f), \tag{9}$$

because for coherent evolution the Hamiltonian is hermitian and the propagator is unitary, $\mathbf{U}^{-1}(t_f, t_i) = \mathbf{U}^{\dagger}(t_f, t_i)$. In the interaction representation the propagator belongs to the SU (2) group and can be parameterized by the Cayley–Klein parameters [7] a and b as

$$\mathbf{U}(t_f, t_i) = \begin{bmatrix} a & -b^* \\ b & a^* \end{bmatrix}. \tag{10}$$

Therefore, the transition probability from t_i to t_f is $P^{if}_{1\to 2} = |b|^2$, and the transition probability from t_f to t_i is $P^{fi}_{1\to 2} = |-b|^2 = P^{if}_{1\to 2}$; hence the forward and backward transition probabilities are equal.

This property holds only when: (i) there are only two states (only then the off-diagonal Cayley–Klein parameters are equal in absolute value, Eq. (10)); (ii) there are no incoherent processes (only then Eq. (9) holds). When there are incoherent processes, or/and more than two states, the forward and backward transition probabilities generally differ. For example, in stimulated Raman adiabatic passage (STIRAP) [8], the forward (with counterintuitive pulse order) and backward (with intuitive order) processes lead to substantially different results.

3.2. Chirped-pulse excitation

Chirped laser pulses introduce further symmetries and asymmetries in two-state excitation.

3.2.1. Lossless case ($\Gamma = 0$)

3.2.1.1. Symmetric pulse shape. In the lossless case ($\Gamma = 0$), when all terms but the chirp are even functions of time and the chirp is an odd function of time, Eqs. (3), (4) and (7), the sign flip of the chirp is equivalent to a time inversion; then if the up-chirp corresponds to the forward process, the down-chirp corresponds to the backward process. An example is shown in Fig. 2 where the Rabi frequency and the energies (diabatic and adiabatic) are plotted together with the time evolution of the populations in the absence of losses ($\Gamma = 0$). The pulsed field creates an avoided crossing of the adiabatic (dressed) energies. The sign of the chirp (up-chirp or down-chirp) determines when the crossing occurs: at early (for up-chirp) or late (for down-chirp) times. The final transition probability is the same for up and down chirps because of the symmetries discussed above. However, the population histories are different and this makes a difference when a population loss mechanism is present, such as ionization induced by the excitation pulse. Then an *early* crossing will expose *more* population to ionization and therefore will produce a *larger* ionization signal. The presence or absence of ac Stark shift does not alter qualitatively the picture in this case.

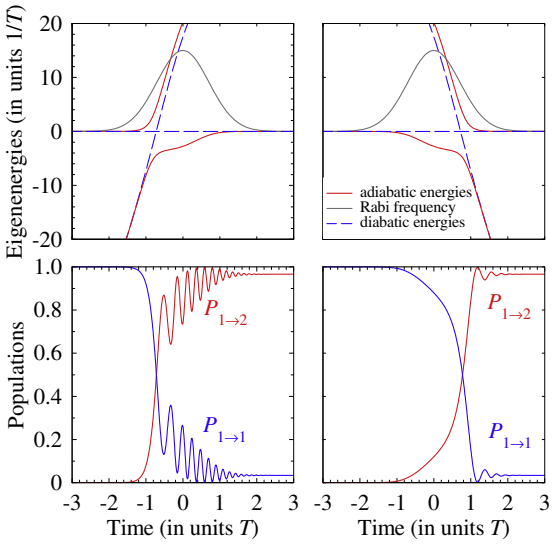

Fig. 2. The Rabi frequency and the energies in a two-state system (upper plots) and the populations (bottom plots) for a symmetric Gaussian pulse (7a) with a peak Rabi frequency $\Omega_0 = 15/T$, for a linear chirp (5), with static detuning $\Delta_0 = 10/T$, relative Stark shift $s = 0.5$, and no population loss ($\Gamma = 0$). Left frames: up-chirp, $C = 20/T^2$, right frames: down-chirp, $C = -20/T^2$.

By combining arguments from the above discussion it is readily seen that the populations are invariant to the sign change of the symmetric part $\Delta_e(t)$ of the detuning, e.g., the static part Δ_0 for zero Stark shift. Indeed, the sign change $\Delta_e(t) \to -\Delta_e(t)$ is equivalent to the combination of the two sign changes $\Delta_o(t) \to -\Delta_o(t)$ and $\Delta(t) \to -\Delta(t)$, which, as we showed above, do not change the post-pulse populations. The implication is that the excitation line profile $P_{1\to 2}(\Delta_0)$ is a symmetric function (in the absence of Stark shift), even in the presence of a frequency chirp.

3.2.1.2. Asymmetric pulse shape. If the pulse shape is asymmetric in time, the sign flip of the chirp is *not* equivalent to time inversion and the transition probabilities for up-chirp and down-chirp may differ. This is easily understood from another viewpoint, when the chirp is sufficiently large to create an energy level crossing (at time t_c): for an asymmetric pulse, an up-chirp can create a level crossing at different value of the Rabi frequency than does a down-chirp; hence the transition probabilities, which depend primarily on the ratio $\Omega(t_c)^2/|C|$, will differ in general [9].

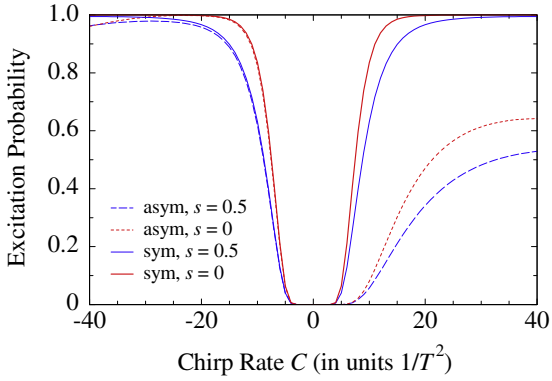

Fig. 3. Excitation probability vs. the chirp rate C in the absence of losses ($\Gamma = 0$). The four curves represent combinations of presence ($s = 0.5$) or absence ($s = 0$) of Stark shift, and symmetric (sym) or asymmetric (asym) pulse shapes. The peak Rabi frequency is $\Omega_0 = 15/T$ and the static detuning is $\Delta_0 = 10/T$.

Fig. 3 illustrates these properties for symmetric and asymmetric pulse shapes, in the presence and absence of ac Stark shift, and for linear chirp. The figure shows that the chirp asymmetry occurs only for asymmetric pulse shape (7b). The presence of ac Stark shift (whenever present it is assumed quite strong, $S_0 = 0.5\Omega_0$) has only a marginal effect. The very small value of the excitation probability around zero chirp is due to the large static detuning Δ_0.

3.2.2. Lossy case ($\Gamma > 0$)

The presence of ionization loss breaks the symmetry of the Hamiltonian (2). Then even if the pulse shape $f(t)$ is symmetric the ionization probability $P_{\rm ion}$ exhibits asymmetry with respect to the sign of the chirp C. This is demonstrated in Fig. 4. The only case when $P_{\rm ion}$ is symmetric vs C is when the static detuning and the ac Stark shift both vanish, $\Delta_0 = 0$ and $S_0 = 0$; then the change of sign of the chirp is equivalent to sign inversion of the detuning, with no effect on the probabilities. Similar asymmetry as in $P_{\rm ion}$ emerges in the excitation probability $P_{1\to 2}$.

It is far less evident that the *survival* probability $P_{1\to 1}$ *retains* its symmetry versus the chirp, even though $P_{\rm ion}$ and $P_{1\to 2}$ are asymmetric. It is shown in Appendix A that if the Rabi frequency $\Omega(t)$ and the loss rate $\Gamma(t)$ are even functions of time, while the detuning is a sum of an even part $\Delta_{\rm e}$ (the static component and the Stark shift) and an odd part $\Delta_{\rm o}$ (the chirp component), then changing the sign of the odd (or the even) part leaves the final survival probability unchanged, although the evolution can be different. The implication is that the survival probability $P_{1\to 1}$ is an even function of the chirp rate C (regardless of the Stark shift). The survival probability $P_{1\to 1}$ is an even function of the static detuning Δ_0 only in the absence of Stark shift ($s = 0$), because the symmetric part of the detuning $\Delta_{\rm e}$ is a sum of the static detuning and the Stark shift. With nonzero Stark shift, the symmetry is lost and $P_{1\to 1}$ is asymmetric vs. Δ_0.

These features are illustrated in Fig. 5, which shows a contour plot of the probabilities $P_{1\to 1}$ and $P_{1\to 2}$ and the ionization probability $P_{\rm ion}$ vs. the static detuning Δ_0 and the chirp rate C. The transition probability $P_{1\to 2}$ and the ionization probability $P_{\rm ion}$ are highly asymmetric vs. both Δ_0 and C. Because the pulse shape is symmetric, this asymmetry is caused by the presence of ionization losses. However, the ground-state probability $P_{1\to 1}$ (i.e. the survival probability) is symmetric vs. the chirp C, in complete agreement with the property proved in Appendix A. Because of the absence of Stark shift, $P_{1\to 1}$ is also symmetric vs. Δ_0.

The fact that asymmetry exists follows from the broken symmetries of the Hamiltonian in the presence of losses, as explained above. The details of this asymmetry, e.g., which chirp favours ionization, can be understood by looking at the time evolution of the probabilities and the respective energy diagram. Fig. 6 presents a typical example of time evolution for four different combinations of detunings and chirps. As discussed above, an early crossing induces a larger ionization signal. An early crossing occurs when both the static detuning Δ_0 and the chirp rate C have the same sign, positive (top right frame) or negative (bottom left frame); as expected, the ionization signal in these cases is larger.

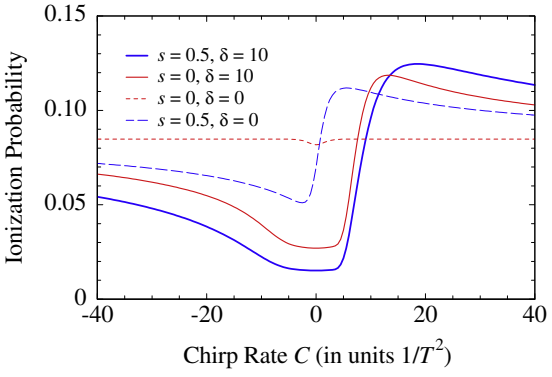

Fig. 4. Ionization probability vs. the chirp rate C in the presence of ionization losses ($\Gamma_0 = 0.1/T$). The four curves represent combinations of presence or absence of Stark shift and static detuning, for symmetric pulse shapes. The peak Rabi frequency is $\Omega_0 = 15/T$.

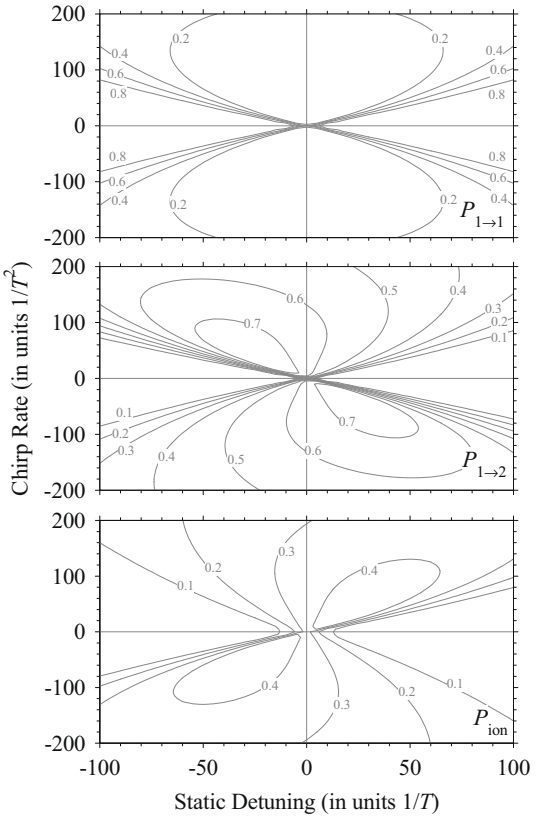

Fig. 5. Probabilities $P_{1\to 1}$ and $P_{1\to 2}$ and the ionization probability $P_{\rm ion}$ vs. the static detuning Δ_0 and the chirp rate C in the presence of ionization losses ($\Gamma_0 = 0.5/T$) and in the absence of Stark shift, $s = 0$. The pulse shape is Gaussian, Eq. (7a), with a peak Rabi frequency $\Omega_0 = 15/T$.

4. Analytic models

Now we shall present two exactly soluble analytic models, which will allow us to illustrate explicitly the features discussed above.

4.1. Generalized Demkov–Kunike model

The generalized Demkov–Kunike (DK) model is defined by

$$\Omega(t) = \Omega_0\ \mathrm{sech}(t/T), \quad \Delta(t) = \Delta_0 + B\tanh(t/T), \tag{11}$$

where Ω_0, Δ_0 and B are real parameters and the loss rate of the excited state is $\Gamma(t) = \Gamma_0 = \mathrm{const} \geqq 0$. Because of the constant population loss this model is suitable to describe excitation in the presence of fluorescence from the excited state to other states outside the system, or in the presence of ionization from the excited state induced by another, cw laser, coupling this state to the continuum. In the original DK model, there is no population loss, $\Gamma_0 = 0$ [2]. By following the derivation in [10] we can solve the generalized DK model for $\Gamma_0 \geqq 0$. The exact survival probability (the ground-state population) at $t \to \infty$ is [10]

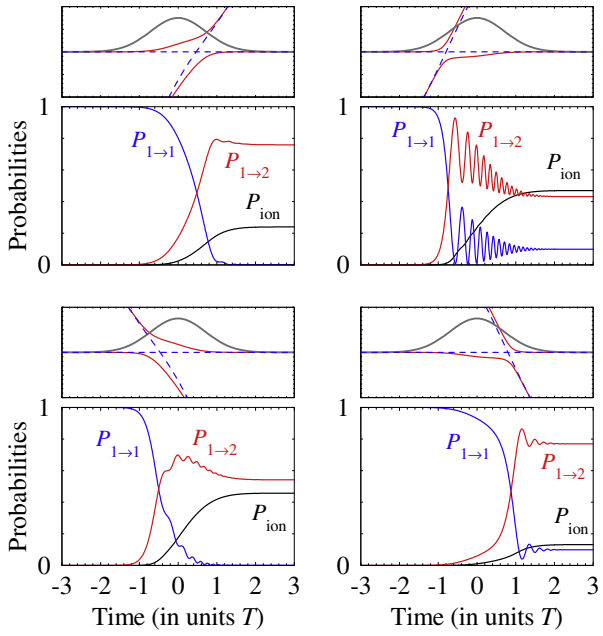

Fig. 6. Time evolution of the probabilities $P_{1\to1}$ and $P_{1\to2}$ and the ionization probability $P_{\rm ion}$ in the presence of ionization losses ($\Gamma_0 = 0.5/T$) and ac Stark shift, $s = 0.5$. The pulse shape is a Gaussian, with a peak Rabi frequency $\Omega_0 = 15/T$. The four frames correspond to four combinations of positive and negative Δ_0 and C: (i) upper left: $\Delta_0 = -20/T$, $C = 30/T^2$; (ii) upper right: $\Delta_0 = 20/T$, $C = 30/T^2$; (iii) lower left: $\Delta_0 = -20/T$, $C = -30/T^2$; (iv) lower right: $\Delta_0 = 20/T$, $C = -30/T^2$. On the top of each frame with the probabilities, the corresponding energy diagram is displayed. Thin solid curves show the adiabatic (dressed) energies, the dashed curves show the diabatic energies, and the thick curves the laser pulse envelope.

$$P_{1\to1} = \left| \frac{\Gamma\left[\frac{1}{2}\left(1+\frac{1}{2}\gamma + i(\delta-\beta)\right)\right]\Gamma\left[\frac{1}{2}\left(1+\frac{1}{2}\gamma + i(\delta+\beta)\right)\right]}{\Gamma\left[\frac{1}{2}\left(1+\frac{1}{2}\gamma + \varkappa + i\delta\right)\right]\Gamma\left[\frac{1}{2}\left(1+\frac{1}{2}\gamma - \varkappa + i\delta\right)\right]} \right|^2, \tag{12}$$

with $\alpha = \Omega_0 T$, $\beta = BT$, $\gamma = \Gamma_0 T$, $\delta = \Delta_0 T$ and $\varkappa = \sqrt{\alpha^2 - \beta^2}$. In the absence of decay, when $\gamma = 0$, this probability coincides with the original DK probability [2]:

$$P_{1\to1} = \frac{\cosh(\pi\delta) + \cos(\pi\varkappa)}{\cosh(\pi\delta) + \cosh(\pi\beta)}. \tag{13}$$

The transition probability $P_{1\to2}$ vanishes as $t \to \infty$ because of the constant loss, $P_{1\to2} \to 0$. The ionization is

$$P_{\rm ion} = 1 - P_{1\to1}. \tag{14}$$

Eqs. (12) and (14) show that the survival probability $P_{1\to1}$ and the ionization $P_{\rm ion}$ are symmetric versus the signs of Δ_0 and B, as expected from the general theory in Section 3. This property is illustrated in Fig. 7, where the survival and ionization probabilities are plotted versus the static detuning Δ_0 and the chirp rate B.

4.2. Generalized Carroll–Hioe model

4.2.1. The model

Another exactly soluble analytic model is defined by

$$\Omega(t) = \Omega_0 \ \mathrm{sech}(t/T), \tag{15a}$$
$$\Delta(t) = B\tanh(t/T) + S_0 \ \mathrm{sech}(t/T). \tag{15b}$$

When Ω_0, B, and S_0 are real the solution has been derived by Carroll and Hioe (CH) [3]. Here we extend this model to nonzero loss rate:

$$\Gamma(t) = \Gamma_0 \ \mathrm{sech}(t/T); \tag{16}$$

the exact solution is derived in Appendix B. This model allows us to describe two-photon excitation with a tanh chirp, in the presence of ac Stark shift and single-photon ionization. Because the Rabi frequency, the Stark shift and the population loss rate are all proportional to the same function sech(t), this model is particularly suitable for two-photon excitation with simultaneous single-photon ionization; then the CH model imposes a hyperbolic-secant temporal dependence on the intensity of the laser pulse.

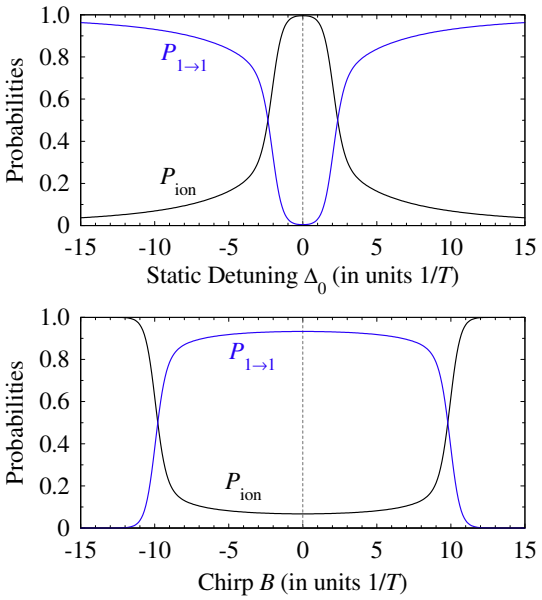

Fig. 7. Survival probability $P_{1\to1}$ and ionization $P_{\rm ion}$ for the Demkov–Kunike model vs. the static detuning δ (for $\alpha = 10, \beta = 2, \gamma = 0.2$) (top) and the chirp β (for $\alpha = 10, \delta = 10, \gamma = 0.2$) (bottom).

4.2.2. Transition probabilities: exact

The transition probabilities are derived in Appendix B and read:

$$P_{1\to1} = \mathrm{e}^{-\pi\gamma}\left|\frac{\mathrm{e}^{\pi\beta/2}\cos 2\pi q - \mathrm{e}^{-\pi\beta/2}\cos 2\pi r}{\sinh\pi\beta}\right|^2, \tag{17a}$$

$$P_{1\to2} = \mathrm{e}^{-\pi\gamma}\left(\frac{\pi^2\alpha\beta}{2\sinh\pi\beta}\right)^2 \times |\Gamma(1-i\beta/2+r+q)\Gamma(1-i\beta/2+r-q)|^{-2} \times |\Gamma(1-i\beta/2-r+q)\Gamma(1-i\beta/2-r-q)|^{-2}, \tag{17b}$$

$$P_{2\to1} = \mathrm{e}^{-\pi\gamma}\left(\frac{\pi^2\alpha\beta}{2\sinh\pi\beta}\right)^2 \times |\Gamma(1+i\beta/2+r+q)\Gamma(1+i\beta/2+r-q)|^{-2} \times |\Gamma(1+i\beta/2-r+q)\Gamma(1+i\beta/2-r-q)|^{-2}, \tag{18a}$$

$$P_{2\to2} = \mathrm{e}^{-\pi\gamma}\left|\frac{\mathrm{e}^{-\pi\beta/2}\cos 2\pi q - \mathrm{e}^{\pi\beta/2}\cos 2\pi r}{\sinh\pi\beta}\right|^2, \tag{18b}$$

where

$$r = \frac{1}{4}\sqrt{\alpha^2 + (\sigma + i\beta - i\gamma)^2}, \tag{19a}$$

$$q = \frac{1}{4}\sqrt{\alpha^2 + (\sigma - i\beta - i\gamma)^2}, \tag{19b}$$

with $\alpha = \Omega_0 T$, $\beta = BT$, $\gamma = \Gamma_0 T$, and $\sigma = S_0 T$. It is easy to verify that for $\gamma = 0$ we have $P_{1\to1} = P_{2\to2}$ and $P_{1\to2} = P_{2\to1}$ because $r = q^*$. For $\gamma \neq 0$ these equalities do not hold.

For a system initially in state 1, the ionization signal is

$$P_{\rm ion} = 1 - P_{1\to1} - P_{1\to2}. \tag{20}$$

Obviously, the survival probabilities $P_{1\to1}$ and $P_{2\to2}$, Eqs. (17a) and (18b), are even functions of B and S_0, as it follows also from the general theory. The transition probabilities $P_{1\to2}$ and

$P_{2\to1}$, however, are not invariant upon the sign flip $B \to -B$ or $S_0 \to -S_0$. We illustrate this property in Fig. 8, where the populations and the ionization are plotted vs. the chirp rate B. The survival probability $P_{1\to1}$ is an even function of B, whereas the transition probability $P_{1\to2}$ and the ionization $P_{\rm ion}$ are asymmetric vs. B.

In the absence of Stark shift and losses, $S_0 = \Gamma_0 = 0$, the Carroll–Hioe model reduces to the *Allen–Eberly model*, the transition probability for which reads [11]:

$$P_{1\to2}^{\rm AE} = P_{2\to1}^{\rm AE} = 1 - \frac{\cos^2(\pi\varkappa/2)}{\cosh^2(\pi\beta/2)}, \tag{21}$$

where $\varkappa = \sqrt{\alpha^2 - \beta^2}$. For a sufficiently large chirp rate B and peak Rabi frequency Ω_0, this transition probability approaches unity:

$$P_{1\to2}^{\rm AE} \to 1 \quad (\Omega_0 \gtrsim B \gtrsim 1/T); \tag{22}$$

this is an example of chirped-pulse adiabatic passage [12].

4.2.3. Transition probabilities: asymptotics

The extension of the Carroll–Hioe model to complex parameters presented above allows us to study quantitatively how adiabatic passage is affected by the presence of Stark shift and irreversible ionization losses.

We are interested primarily in the regime of *small* values of σ and γ, $|\sigma - i\gamma| \ll 1$. We use the expansions:

$$r \sim \frac{\varkappa}{4} + \frac{\beta(\gamma + i\sigma)}{4\varkappa} + \mathcal{O}\left(|\sigma - i\gamma|^2\right), \tag{23a}$$

$$q \sim \frac{\varkappa}{4} - \frac{\beta(\gamma + i\sigma)}{4\varkappa} + \mathcal{O}\left(|\sigma - i\gamma|^2\right). \tag{23b}$$

and expand the sine and cosine in Eq. (17a) to find the following asymptotics of the survival probability:

$$P_{1\to1} \sim P_{1\to1}^{\rm AE} e^{-\pi\gamma}\left[1 + \pi\gamma\frac{\beta}{\varkappa}\frac{\tan(\pi\varkappa/2)}{\tanh(\pi\beta/2)} + \mathcal{O}(\sigma^2, \gamma^2)\right]. \tag{24}$$

For the transition probability we find from Eq. (17b) the asymptotics:

$$P_{1\to2} \sim P_{1\to2}^{\rm AE} e^{-\pi\gamma}\left[1 + \mathcal{O}(\sigma^2, \gamma^2)\right]. \tag{25}$$

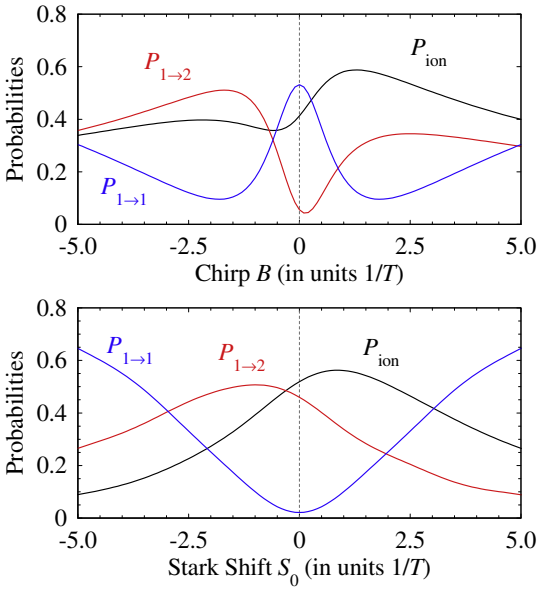

Fig. 8. Probabilities $P_{1\to1}$, $P_{1\to2}$ and the ionization $P_{\rm ion}$ for the Carroll–Hioe model as a function of the chirp rate β (for $\alpha = 2$, $\sigma = 1$, $\gamma = 0.5$) (top) and the Stark shift σ (for $\alpha = 2$, $\beta = 2$, $\gamma = 0.5$) (bottom).

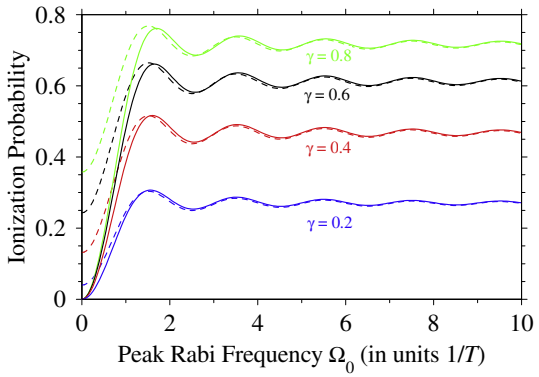

Fig. 9. Ionization in the Carroll–Hioe model as a function of the peak Rabi frequency Ω_0 for different values of the ionization rate $\gamma = \Gamma_0 T$. The chirp rate is $BT = 0.5$ and the Stark shift is $S_0 = 0.1\Omega_0$. The solid curves show the exact values, calculated numerically, and the dashed curves present the asymptotics (26).

Eqs. (24) and (25) show that the Stark shift affects the probabilities only in second order $\mathcal{O}(\sigma^2)$. If $\varkappa = 0$ (i.e. for $\alpha = \beta$), it can be shown that Eqs. (24) and (25) hold up to first order $\mathcal{O}(\sigma, \gamma)$.

Using Eqs. (24) and (25) we obtain the asymptotics of the ionization signal:

$$P_{\rm ion} \sim 1 - e^{-\pi\gamma} - e^{-\pi\gamma}\pi\gamma\frac{\beta}{\varkappa}\frac{\sin(\pi\varkappa)}{\sinh(\pi\beta)} + \mathcal{O}(\sigma^2, \gamma^2). \tag{26}$$

This formula reveals a curious feature of the ionization signal: it exhibits damped oscillations versus the peak Rabi frequency (through $\varkappa$). This feature is indeed intriguing because the unstructured ionization continuum is usually seen as an incoherent medium, void of interference patterns and oscillations. Here we find that the oscillation frequency depends only on $\varkappa = \sqrt{\alpha^2 - \beta^2} \equiv T\sqrt{\Omega_0^2 - B^2}$, i.e. on the peak Rabi frequency Ω_0 and the chirp rate B, but not on the Stark shift S_0 and the decay rate Γ_0. The amplitude of the oscillations depends on all these parameters but S_0; most notably, it vanishes rapidly with the decay rate Γ_0 and the chirp rate B, but only slowly with Ω_0, as a sinc function.

These features are illustrated in Fig. 9, where the ionization signal is plotted versus the peak Rabi frequency for different sets of parameters. When the loss rate Γ_0 is increased the ionization oscillates around an increased asymptotic value, $1 - e^{-\pi\gamma}$, and the oscillation amplitude varies as $\gamma e^{-\pi\gamma}$ (the maximum amplitude is for $\gamma = 1/\pi$), but the phase of the ionization oscillations is almost unaffected. Finally, as follows from Eq. (26), the oscillation amplitude decreases with the chirp rate B, and it is maximal at zero chirp.

5. Conclusion

In this work we have presented a detailed study of the effects of Stark shift and irreversible population loss (ionization) upon chirped adiabatic passage in a two-state quantum system. We have shown that in the presence of population loss channel, various symmetries that exist in the lossless case are broken, whereas others remain intact. We have shown that three conventional detection signals — the post-excitation populations of states 1 and 2 and the ionization signal collected during the excitation — exhibit different symmetries. In particular, the post-excitation population of the initial state (the survival probability) retains its symmetry with respect to sign flip of the even part (typically the static detuning) or the odd part (typically the chirp) of the detuning. The post-excitation population of the other state and the ionization signal, though, do not have this symmetry, and are therefore asymmetric with respect to the chirp and the static detuning.

These features can be observed in a single-photon transition between two states, in which the upper state is ionized by the excitation pulse. A three-state ladder system, with a far-off-resonance intermediate state (which can be eliminated adiabatically), provides another convenient playground for testing these symmetries; For example, the ladder 3s–3p–4s in sodium atom appears particularly suitable [6].

We have made use of two exactly soluble analytic models, which are extensions of the models of Demkov–Kunike and Carroll–Hioe to complex parameters. Both models assume a hyperbolic-secant time dependence of the Rabi frequency. The Demkov–Kunike detuning is a sum of a constant term, the real part of which describes a static detuning and the imaginary part a constant probability loss, and a hyperbolic-tangent chirp. The Carroll–Hioe detuning is a sum of a hyperbolic-secant term, the real part of which describes a Stark shift and the imaginary part an ionization (both caused by the excitation pulse), and a hyperbolic-tangent chirp. This model therefore can be used to describe a two-photon excitation accompanied by simultaneous single-photon ionization.

The analytic solutions make it possible, besides illustrating explicitly the symmetries in the signals, to derive the corrections to the adiabatic passage solution introduced by the Stark shift and the population loss. We have found an interesting oscillatory behavior in the ionization signal. The phase of these oscillations depends primarily on the Rabi frequency, and to a lesser extend on the chirp, but not on the loss rate or the Stark shift. We have used the generalized Carroll–Hioe solution to establish the optimal conditions for experimental observation.

Acknowledgments

This work has been supported by the European Commission projects EMALI and FASTQUAST, and the Bulgarian NSF, Grant Nos. VU-I-301/07 D002-90/08, IRC-CoSiM and Sofia University, Grant No. 020/2009.

Appendix A. Invariances of the survival probabilities

We show here, that the survival probabilities $P_{1\to1}$ and $P_{2\to2}$ in a lossy two-state system do not depend on the sign change of the odd part $\Delta_o(t)$ and the even part $\Delta_e(t)$ of the detuning, provided the Rabi frequency $\Omega(t)$ and the loss rate $\Gamma(t)$ are even functions of time. We write the Hamiltonian in the interaction representation:

$$\mathbf{H}(t)=\frac{\hbar}{2}\begin{bmatrix}0 & \Omega(t)e^{-iD(t)}\\ \Omega(t)e^{iD(t)} & 0\end{bmatrix}, \tag{A1}$$

with $D(t)=\int_0^t(\Delta(t')-i\Gamma(t')/2)dt'$. The formal solution for the evolution operator is expressed using the Dyson series:

$$\mathbf{U}(\infty,-\infty)=1+\sum_{n=1}^{\infty}\mathbf{U}_n(\infty,-\infty), \tag{A2}$$

where

$$\mathbf{U}_n(\infty,-\infty)=\left(\frac{-i}{\hbar}\right)^n\int_{-\infty}^{\infty}\mathrm{d}t_1\int_{-\infty}^{t_1}\mathrm{d}t_2\cdots\int_{-\infty}^{t_{n-1}}\mathrm{d}t_n \times\mathbf{H}(t_1)\mathbf{H}(t_2)\cdots\mathbf{H}(t_n), \tag{A3}$$

and $t_1>t_2>\cdots>t_n$. It is straightforward to show that the even powers of the Hamiltonian in the sum in Eq. (A2) generate diagonal matrices, while the odd powers are anti-diagonal matrices. We consider the diagonal elements first. Let us examine the simplest diagonal term in the Dyson series, which for $n=2$ reads:

$$\mathbf{U}_2(\infty,-\infty)=-\frac{1}{4}\int_{-\infty}^{\infty}dt_1\int_{-\infty}^{t_1}dt_2\times\begin{bmatrix}\Omega_1\Omega_2e^{-i(D_1-D_2)} & 0\\ 0 & \Omega_1\Omega_2e^{i(D_1-D_2)}\end{bmatrix}. \tag{A4}$$

The subscripts in Ω_k and D_k indicate the instant of time t_k. The higher powers of the Hamiltonian in the Dyson series have a similar simple form.

By using simple transformations of variables, it can be shown that $\mathbf{U}_2(\infty,-\infty)$ is invariant under the transformation $\Delta_o\leftrightarrow-\Delta_o$, while the change $\Delta_e\leftrightarrow-\Delta_e$ leads only to complex conjugation. These results are also valid for the higher even-order terms of the Dyson series, which means that the considered transformations do not change the absolute values of the diagonal elements of the evolution matrix. This, in turn, proves the invariance of the survival probabilities.

These arguments obviously do not hold for the odd terms in the sum, which means that in the presence of losses $\Gamma>0$ the transition probabilities $P_{1\to2}$ and $P_{2\to1}$ are *not* invariant with respect to the sign flips $\Delta_o\leftrightarrow-\Delta_o$ and $\Delta_e\leftrightarrow-\Delta_e$.

Appendix B. Solution of the Carroll–Hioe model for complex parameters

In order to solve the Carroll–Hioe model (15), we begin with a phase transformation of the probability amplitudes:

$$c_1(t)\to c_1(t),\quad c_2(t)\to c_2(t)\exp\left[-i\int_0^t\Delta(\tau)d\tau\right], \tag{B1}$$

which brings Eq. (1) into the interaction representation:

$$i\frac{d}{dt}c_1(t)=\frac{1}{2}\Omega(t)e^{-iD(t)}c_2(t), \tag{B2a}$$

$$i\frac{d}{dt}c_2(t)=\frac{1}{2}\Omega(t)e^{iD(t)}c_1(t), \tag{B2b}$$

where $D=\int_0^t\Delta(\tau)d\tau$, i.e.

$$D=(S_0-i\Gamma_0)T\arctan[\sinh(t/T)]+BT\ln[\cosh(t/T)]. \tag{B3}$$

We now change the independent variable from t to z [3]:

$$z=\frac{\sinh(t/T)-i}{\sinh(t/T)+i}, \tag{B4}$$

and denote $C_n(z)=c_n(t(z))$ $(n=1,2)$. As t changes from $-\infty$ to ∞, the variable z changes from 1 to $e^{2\pi i}$. By following the derivation of Carroll and Hioe [3], we obtain the following solution for $C_1(z)$ in terms of the Gauss hypergeometric function $F(a,b;c;z)$ [13]:

$$C_1(z)=z^{-r-(\sigma-i\gamma+i\beta)/4}\times\Big[Az^{2r}F(-i\beta/2+r+q,-i\beta/2+r-q;1+2r;z) +BF(-i\beta/2-r+q,-i\beta/2-r-q;1-2r;z)\Big], \tag{B5}$$

where

$$r=\frac{1}{4}\sqrt{\alpha^2+(\sigma+i\beta-i\gamma)^2}, \tag{B6a}$$

$$q=\frac{1}{4}\sqrt{\alpha^2+(\sigma-i\beta-i\gamma)^2}, \tag{B6b}$$

and

$$\alpha=\Omega_0T,\quad \sigma=S_0T,\quad \gamma=\Gamma_0T,\quad \beta=BT. \tag{B7}$$

The integration constants A and B can be determined from the initial conditions $c_1(-\infty)=1$, $c_2(-\infty)=0$:

$$A=\frac{\Gamma(-i\beta)\Gamma(-2r)}{\Gamma(-r+q-i\beta/2)\Gamma(-r-q-i\beta/2)}, \tag{B8a}$$

$$B=\frac{\Gamma(-i\beta)\Gamma(2r)}{\Gamma(r+q-i\beta/2)\Gamma(r-q-i\beta/2)}. \tag{B8b}$$

Then the solution for $C_1(z)$ reads:

$$C_1(z) = z^{-(\sigma - i\gamma + i\beta)/4} \times \Big[z^{-r} \frac{\Gamma(-i\beta)\Gamma(2r)}{\Gamma(-i\beta/2 + r + q)\Gamma(-i\beta/2 + r - q)} \times F(-i\beta/2 - r + q, -i\beta/2 - r - q; 1 - 2r; z) + z^{r} \frac{\Gamma(-i\beta)\Gamma(-2r)}{\Gamma(-i\beta/2 - r + q)\Gamma(-i\beta/2 - r - q)} \times F(-i\beta/2 + r + q, -i\beta/2 + r - q; 1 + 2r; z) \Big]. \quad \text{(B9)}$$

In a similar manner we derive the solution for the probability amplitude $C_2(z)$, by using Eq. (B2a):

$$C_2(z) = -\frac{\alpha}{4} 2^{i\beta} z^{(\sigma - i\gamma + i\beta)/4 - r} e^{\pi(\beta - i\sigma + \gamma)/2} \times \Big[\frac{\Gamma(1 - i\beta)\Gamma(2r)}{\Gamma(1 - i\beta/2 + r + q)\Gamma(1 - i\beta/2 + r - q)} \times F(i\beta/2 - r + q, i\beta/2 - r - q; 1 - 2r; z) + z^{2r} \frac{\Gamma(1 - i\beta)\Gamma(-2r)}{\Gamma(1 - i\beta/2 - r + q)\Gamma(1 - i\beta/2 - r - q)} \times F(i\beta/2 + r + q, i\beta/2 + r - q; 1 + 2r; z) \Big]. \quad \text{(B10)}$$

From Eqs. (B9) and (B10), and recalling the transformation (B1), one can derive the propagator elements U_{11} and U_{21} in the original basis by using the Gauss summation formula:

$$F(a, b; c; 1) = \frac{\Gamma(c - a + b)\Gamma(c)}{\Gamma(c - a)\Gamma(c - b)}. \quad \text{(B11)}$$

The result is

$$U_{11}(\infty) = e^{-\pi(i\sigma + \gamma)/2} \frac{e^{\pi\beta/2} \cos 2\pi q - e^{-\pi\beta/2} \cos 2\pi r}{\sinh \pi\beta}, \quad \text{(B12a)}$$

$$U_{21}(\infty) = -i \frac{\pi\alpha}{2} 2^{i\beta} (\cosh t_f)^{-i\beta} e^{-\pi(\gamma + i\sigma)/2} \Gamma(1 - i\beta)^2 \times [\Gamma(1 - i\beta/2 + r + q)\Gamma(1 - i\beta/2 + r - q) \times \Gamma(1 - i\beta/2 - r + q)\Gamma(1 - i\beta/2 - r - q)]^{-1}. \quad \text{(B12b)}$$

In a similar fashion, we can derive the solution for the model (15) for the initial conditions $c_1(-\infty) = 0$, $c_2(-\infty) = 1$, which will give us the propagator elements U_{12} and U_{22}. We use that Eqs. (B2) are of the same form as for initial conditions $c_1(-\infty) = 1$, $c_2(-\infty) = 0$, but for $\Delta \to -\Delta$, i.e. $\beta \to -\beta$, $\sigma \to -\sigma$, $\gamma \to -\gamma$, $r \to r$, $q \to q$. By using Eqs. (B1) and (B3) we obtain:

$$U_{12}(\infty) = -i \frac{\pi\alpha}{2} 2^{-i\beta} (\cosh t_f)^{i\beta} e^{-\pi(\gamma + i\sigma)/2} \Gamma(1 + i\beta)^2 \times [\Gamma(1 + i\beta/2 + r + q)\Gamma(1 + i\beta/2 + r - q) \times \Gamma(1 + i\beta/2 - r + q)\Gamma(1 + i\beta/2 - r - q)]^{-1}, \quad \text{(B13a)}$$

$$U_{22}(\infty) = e^{-\pi(i\sigma + \gamma)/2} \frac{e^{\pi\beta/2} \cos 2\pi r - e^{-\pi\beta/2} \cos 2\pi q}{\sinh \pi\beta}. \quad \text{(B13b)}$$

The transition probabilities $P_{m \to n} = |U_{nm}(e^{2\pi i})|^2$ are given explicitly by Eqs. (17) and (18).

References

[1] B.W. Shore, The Theory of Coherent Atomic Excitation, Wiley, New York, 1990.
[2] Y.N. Demkov, M. Kunike, Vestn. Leningr. Univ. Fiz. Khim. 16 (1969) 39;
F.T. Hioe, C.E. Carroll, Phys. Rev. A 32 (1985) 1541;
J. Zakrzewski, Phys. Rev. A 32 (1985) 3748.
[3] C.E. Carroll, F.T. Hioe, J. Phys. A: Math. Gen. 19 (1986) 3579.
[4] J.S. Melinger, A. Hariharan, Suketu R. Gandhi, W.S. Warren, J. Chem. Phys. 95 (1991) 2210;
B. Broers, H.B. van Linden van den Heuvell, L.D. Noordam, Phys. Rev. Lett. 69 (1992) 2062;
C. Trallero-Herrero, D. Cardoza, T.C. Weinacht, J.L. Cohen, Phys. Rev. A 71 (2005) 013423;
S.D. Clow, C. Trallero-Herrero, T. Bergeman, T. Weinacht, Phys. Rev. Lett. 100 (2008) 233603;
C. Trallero-Herrero, J.L. Cohen, T. Weinacht, Phys. Rev. Lett. 96 (2006) 063603.
[5] M. Wollenhaupt et al., Springer Handbook of Lasers and Optics, Springer, 2007. Chapter 12;
M. Wollenhaupt, V. Engel, T. Baumert, Annu. Rev. Phys. Chem. 56 (2005) 25;
M. Wollenhaupt, A. Prakelt, C. Sarpe-Tudoran, D. Liese, T. Bayer, T. Baumert, Phys. Rev. A 73 (2006) 063409;
T. Bayer, M. Wollenhaupt, C. Sarpe-Tudoran, T. Baumert, Phys. Rev. Lett. 102 (2009) 023004.
[6] A. Präkelt, M. Wollenhaupt, C. Sarpe-Tudoran, T. Baumert, Phys. Rev. A 70 (2004) 063407;
M. Krug, T. Bayer, M. Wollenhaupt, C. Sarpe-Tudoran, T. Baumert, S.S. Ivanov, N.V. Vitanov, New J. Phys. 11 (2009) 105051.
[7] D.A. Varshalovich, A.N. Moskalev, V.K. Khersonskii, Quantum Theory of Angular Momentum, World Scientific, Singapore, 1988.
[8] U. Gaubatz, P. Rudecki, S. Schiemann, K. Bergmann, J. Chem. Phys. 92 (1990) 5363;
S. Schiemann, A. Kuhn, S. Steuerwald, K. Bergmann, Phys. Rev. Lett. 71 (1993) 3637;
N.V. Vitanov, M. Fleischhauer, B.W. Shore, K. Bergmann, Adv. Atom. Mol. Opt. Phys. 46 (2001) 55.
[9] L.D. Landau, Phys. Z. Sowjetunion 2 (1932) 46;
C. Zener, Proc. R. Soc. Lond. A 137 (1932) 696;
E.C.G. Stückelberg, Helv. Phys. Acta 5 (1932) 369.
[10] N.V. Vitanov, S. Stenholm, Phys. Rev. A. 55 (1997) 2982.
[11] L. Allen, J.H. Eberly, Optical Resonance and Two-Level Atoms, Dover, New York, 1987;
F.T. Hioe, Phys. Rev. A 30 (1984) 2100.
[12] N.V. Vitanov, T. Halfmann, B.W. Shore, K. Bergmann, Annu. Rev. Phys. Chem. 52 (2001) 763.
[13] M. Abramowitz, I.A. Stegun, Handbook of Mathematical Functions, Dover, New York, 1964.